Geometry Optimization in Cooperative Integrated Sensing and Communication Networks

Kaitao Meng*, Kawon Han*, Christos Masouros*, and Lajos Hanzo†
*Department of Electronic and Electrical Engineering, University College London, UK
†School of Electronics and Computer Science, University of Southampton, UK
Emails: *{kaitao.meng, kawon.han c.masouros}@ucl.ac.uk †lh@ecs.soton.ac.uk

***Abstract*—This work studies a cooperative architecture for integrated sensing and communication (ISAC) networks, incorporating coordinated multi-point (CoMP) transmission along with multi-static sensing. We investigate the allocation of antennas-to-base stations (BSs) as a means to optimize antenna densities and explore the range between massive MIMO and cell-free typologies, and their effects on cooperative sensing and cooperative communication performance. Regarding sensing performance, we investigate three localization methods: angle-of-arrival (AOA)-based, time-of-flight (TOF)-based, and a hybrid approach combining both AOA and TOF measurements, to comprehensively assess their effects on ISAC network performance. In networks with multiple ISAC nodes following a Poisson point process, the Cramér-Rao lower bound (CRLB) for time of flight (TOF)-based methods decreases with the square of the logarithm of the number of nodes, for angle of arrival (AOA)-based methods with the logarithm, and for hybrid methods as a mix of both. In terms of communication performance, we derive a tractable expression for the communication data rate under various cooperative region sizes. The proposed cooperative scheme shows superior performance improvement compared to centralized or distributed antenna allocation strategies.**

I. Introduction

Integrated sensing and communication (ISAC) technologies have garnered substantial academic and industrial interest [1], [2]. ISAC is recognized for its ability to leverage unified infrastructure and waveforms to simultaneously transmit information and receive echoes, thereby significantly enhancing the efficiency of spectrum, cost, and energy [3]. While most research focuses on system-level optimizations like waveform design and resource management within individual base stations (BSs) [4], [5], the potential of network-level ISAC, especially multi-cell sensing and communication (S&C) cooperation, remains underexplored.

Network-level ISAC presents distinct advantages over single-cell ISAC, including expanded coverage, enhanced service quality, and more flexible performance tradeoffs [6], [7]. Specifically, with the exploitation of the target-reflected signals over the multistatic links, the sensing capabilities of ISAC can be maximized through multi-static sensing configurations formed by several cooperative BSs. Additionally, advanced coordinated multi-point (CoMP) transmission and reception techniques can be employed to enhance communication performance by connecting a single user to multiple BSs [8]. Some early studies have explored network-level trade-offs between sensing and communication [9], [10].

In ISAC networks, optimal antenna-to-BS allocation, represented by the number of antennas per site, plays a critical role in maximizing the cooperative gains for both sensing and communication, since these two functions have fundamentally different requirements for their antenna configurations. Typically, the antenna-to-BS allocation strategies fall into two main categories: namely centralized and distributed configurations. Centralized multiple input multiple output (MIMO) systems reduce costs by concentrating antennas in a single location within the service region [11]. However, this approach is prone to high spatial channel correlation. By contrast, distributed MIMO configurations, where antennas are dispersed across various locations, can mitigate channel correlation and enhance system performance by reducing targets/users access distances [12], while its primary drawback is the challenge of maintaining precise synchronization across all antennas.

Building on the previous discussions, we propose a cooperative ISAC scheme, as shown in Fig. 1, where multiple BSs within the cooperative communication region cooperatively transmit the same information data to the served user, while another set of BSs within the cooperative sensing region collaborate with the objective of offering localization services for each target. In this work, we investigate three different target localization methods: angle-of-arrival (AOA)-based, time-of-flight (TOF)-based, and a hybrid of AOA and TOF based localization, to comprehensively assess the impact of antenna-to-BS allocation on the cooperative sensing and communication performance of ISAC networks. The main contributions of this paper are summarized as follows:

- We propose a cooperative ISAC network that integrates multi-static sensing with CoMP data transmission. We derive the scaling laws of the CRLB for TOF-based, AOA-based, and hybrid localization methods.
- We derive the effective channel gain and the Laplace transform of both the useful signals and inter-cell interference by utilizing the moment-generating functions. We establish a tractable expression for the communication data rate of various antenna-to-BS allocation strategies.

II. System Model

A. Network Model

In this study, we utilize stochastic geometry tools to derive the expressions of ISAC network performance and optimize the number of antennas allocated at each BS, as shown in

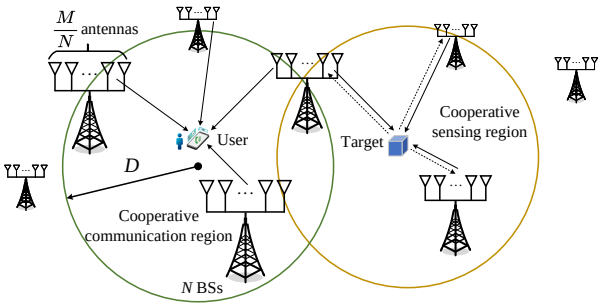

Fig. 1. Illustration of antenna-to-BS allocation in cooperative ISAC networks.

Fig. 1. Specifically, we define antenna density and BS density as the average number of antennas per km^2 and the average number of BS per km^2, respectively. Then, given the transmit antenna density λ_t and receive antenna density λ_r, assuming each BS has a uniform linear array, the BS density to be optimized is denoted by $\lambda_b = \frac{\lambda_t}{M_t} = \frac{\lambda_r}{M_r}$, where M_t and M_r represent the number of transmit and receive antennas per BS, respectively. It is assumed that the locations of BSs follow a homogeneous Poisson point process (PPP) in a two-dimensional space, denoted by $\Phi_b = \{\mathbf{d}_i = [x_i, y_i]^T \in \mathbb{R}^2\}$, where $\mathbf{d}_i$ represents the location of BS i.

As shown in Fig. 1, BSs inside the cooperative region $\mathcal{C} \subset \mathbb{R}^2$, defined by the circle with center at the target/user and radius D, are members of the cluster for cooperative S&C. Specifically, each user is served by multiple BSs within the cooperative region, and these BSs transmit the same signals by forming a non-coherent CoMP cluster. Similarly, BSs within the cooperative region of the target collaborate to provide localization services by forming a distributed non-coherent multi-static radar system, with orthogonal transmission utilizing a code-division multiplexing scheme.

Each BS designs the transmit precoding for sending the information signal s^c to the served user, together with a dedicated radar signal s_i^s for the detected target. $\mathrm{E}[s_i^s (s_i^c)^H] = 0$, this is consistent with the assumptions in [1]. Upon letting $\mathbf{s}_i = [s_i^s, s_i^c]^T$, we have $\mathrm{E}\left[\mathbf{s}_i \mathbf{s}_i^H\right] = \mathbf{I}_2$. Then, the signal transmitted by the ith BS is given by

$$\mathbf{x}_i = \mathbf{W}_i \mathbf{s}_i = \mathbf{w}_i^c s_i^c + \mathbf{w}_i^s s_i^s, \tag{1}$$

where $\mathbf{w}_i^c$ and $\mathbf{w}_i^s \in \mathbb{C}^{M_t \times 1}$ are normalized transmit beamforming vectors, i.e., $\|\mathbf{w}_i^c\|^2 = p^c$ and $\|\mathbf{w}_i^s\|^2 = p^s$. Furthermore, p^s and p^c respectively represent the transmit power of the S&C signals, and $\mathbf{W}_i = [\mathbf{w}_i^c, \mathbf{w}_i^s] \in \mathbb{C}^{M_t \times 2}$ is the transmit precoding matrix of the BS at $\mathbf{d}_i$. To avoid the interference between S&C, we adopt zero-forcing (ZF) beamforming for the sake of making the analysis tractable. Then, the beamforming vector of the serving BS i is given by $\mathbf{W}_i = \tilde{\mathbf{W}}_i / \sqrt{\mathrm{diag}(\tilde{\mathbf{W}}_i^H \tilde{\mathbf{W}}_i)}$, where $\tilde{\mathbf{W}}_i = \mathbf{H}_i \left(\mathbf{H}_i^H \mathbf{H}_i\right)^{-1}$ and $\mathbf{H}_i = [(\mathbf{h}_{i,c}^H)^T, (\mathbf{a}^H(\theta_i))^T]^T$. Here, $\mathbf{h}_{i,c}^H \in C^{M_t \times 1}$ denotes the communication channel spanning from BS i to the typical user, and $\mathbf{a}^H(\theta_i) \in C^{M_t \times 1}$ represents the sensing channel impinging from BS i to the typical target. We have $p^s + p^c = 1$ with normalized transmit power.

B. Cooperative Sensing Model

We aim to explore the optimal antenna-to-BS allocation method by examining the scaling laws of target localization techniques that rely on AOA measurements, TOF measurements, and a combination of both, respectively. The location of a typical target is denoted as $\boldsymbol{\psi}_t = [x_t, y_t]^T$. According to Slivnyak's theorem [13], the typical target is assumed to be located at the origin, and its performance is evaluated as a representative measure of the average performance across all targets in the network, using the probability distribution function of the distances from the BSs to this origin. Assuming unbiased estimations, the CRLB serves as a benchmark for theoretical localization accuracy in terms of the mean squared error (MSE), which can be expressed as

$$\mathrm{var}\{\hat{\boldsymbol{\psi}}_t\} = \mathrm{E}\{|\hat{\boldsymbol{\psi}}_t - \boldsymbol{\psi}_t|^2\} \geq \mathrm{CRLB}, \tag{2}$$

where $\hat{\boldsymbol{\psi}}_t = [\hat{x}_t, \hat{y}_t]^T$ represents the estimated location of the typical target. The typical target is collaboratively sensed by N BSs. Let us assume that the transmitted radar signals $\{s_i^s\}_{i=1}^N$ of the BSs in the cooperative sensing cluster are approximately orthogonal for any time delay of interest [14]. The base-band equivalent of the impinging signal at receiver j is represented as

$$\mathbf{y}_j(t) = \sum\nolimits_{i=1}^{N} \sigma d_j^{-\frac{\beta}{2}} \mathbf{b}(\theta_j)\, d_i^{-\frac{\beta}{2}} \mathbf{a}^H(\theta_i) \mathbf{W}_i \boldsymbol{s}_i + \mathbf{n}_l(t), \tag{3}$$

where $d_i = \|\mathbf{d}_i\|$ denotes the distance from BS i to the origin, $\beta \geq 2$ is the pathloss exponent between the serving BS and the typical target, σ denotes the radar cross section (RCS), $\tau_{i,j}$ is the propagation delay of the link spanning from BS i to the typical target and then to BS j, and $\mathbf{n}_l(t)$ is the additive complex Gaussian noise having zero mean and covariance matrix $\sigma_s^2 \mathbf{I}_{M_r}$. In (3), we have $\mathbf{a}^H(\theta_i) = [1, \cdots, e^{j\pi(M_t-1)\cos(\theta_i)}]$, and $\mathbf{b}(\theta_j) = [1, \cdots, e^{j\pi(M_r-1)\cos(\theta_j)}]^T$, where θ_i denotes the angle of bearing for the i-th BS to the target with respect to the horizontal axis.

1) Angle Measurement Based Localization: By measuring the AOAs of each monostatic link and bi-static link, the target location can be estimated by maximum likelihood estimation (MLE) [15]. For the AOA measurement of the bi-static link from the jth BS to the target and then to the ith BS, we have

$$\hat{\theta}_{i,j} = \tan^{-1} \frac{y_t - y_i}{x_t - x_i} + n_{i,j}^a. \tag{4}$$

In (4), $n_{i,j}^a$ denotes the AOA measurement error, and $n_{i,j}^a \sim \mathcal{N}\left(0, \rho_{i,j}^2\right)$, where $\rho_{i,j}^2 = \frac{6}{\pi^2 \cos^2\theta_i M_r (M_r^2-1) G_t \gamma_{i,j}}$ [16] and $\gamma_{i,j} = \frac{\sigma p^s \gamma_0}{d_i^\beta d_j^\beta}$. Here, G_t is the transmit beamforming gain, and γ_0 represents the channel power at the reference distance of 1 m. Then, the Fisher information matrix (FIM) of estimating the parameter vector $\boldsymbol{\psi}_t$ for the AOA-based MIMO radar considered is equal to

$$\mathbf{F}_{\mathrm{A}} = |\zeta_a|^2 \sum\nolimits_{j=1}^{N} \sum\nolimits_{i=1}^{N} \frac{\cos^2\theta_i}{d_j^2 d_i^2} \begin{bmatrix} \frac{\sin^2\theta_i}{d_i^2} & -\frac{\sin\theta_i \cos\theta_i}{d_i^2} \\ -\frac{\sin\theta_i \cos\theta_i}{d_i^2} & \frac{\cos^2\theta_i}{d_i^2} \end{bmatrix}, \tag{5}$$

where $|\zeta_a|^2 = \pi^2 M_r \left(M_r^2-1\right) G_t \sigma p^s \gamma_0 / 6\sigma_s^2$ [17]. Given the random location of ISAC BSs, the expected CRLB for any unbiased estimator of the target position is given by

$$\mathrm{CRLB_A} = \mathrm{E}_{\Phi_b, G_t}\left[\mathrm{tr}\left(\mathbf{F}_\mathrm{A}^{-1}\right)\right]. \tag{6}$$

In (6), the expectation operation accounts for the randomness in the locations of sensing BSs and the variability in beam power caused by user channel fluctuations.

2) Range Measurement Based Localization: From transmitter j to the target and then to receiver i, the term d_{ij} represents the corresponding distance between the jth transmitter and the ith receiver, which is given by $\hat{d}_{ij} = \sqrt{(x_i - x_t)^2 + (y_i - y_t)^2} + \sqrt{(x_j - x_t)^2 + (y_j - y_t)^2} + n_{ij}^r$, where $n_{i,j}^r \sim \mathcal{N}\left(0, \eta_{i,j}^2\right)$ and $\eta_{ij}^2 = \frac{c^2 \sigma_s^2}{8\pi^2 G_t M_r B^2 \gamma_{ij}}$. Let $a_{ij} = \cos\theta_i + \cos\theta_j$ and $b_{ij} = \sin\theta_i + \sin\theta_j$. Then, the FIM of estimating the parameter vector $\boldsymbol{\psi}_t$ for the TOF-based localization method is equal to

$$\mathbf{F}_\mathrm{R} = |\zeta_r|^2 \sum\nolimits_{i=1}^{N} \sum\nolimits_{j=1}^{N} d_i^{-\beta} d_j^{-\beta} \begin{bmatrix} a_{ij}^2 & a_{ij} b_{ij} \\ a_{ij} b_{ij} & b_{ij}^2 \end{bmatrix}, \tag{7}$$

where we have $|\zeta_r|^2 = \frac{8\pi^2 p^s G_t M_r B^2 \sigma\gamma_0}{c^2 \sigma_s^2}$ [18]. Here, c denotes the speed of light, B^2 represents the squared effective bandwidth, and $|\zeta_r|$ is the common system gain term. Given the random location of ISAC BSs, the expected CRLB for any unbiased estimator of the target position is given by

$$\mathrm{CRLB_R} = \mathrm{E}_{\Phi_b, G_t}\left[\mathrm{tr}\left(\mathbf{F}_\mathrm{R}^{-1}\right)\right]. \tag{8}$$

3) Joint Angle and Range Localization: Incorporating both AOA and TOF measurements, rather than relying solely on one type of AOA or TOF measurement, can significantly enhance the accuracy and reliability of our hybrid localization method. Using both AOA and TOF measurements, the expected CRLB for any unbiased estimator of the target position is given by

$$\mathrm{CRLB_H} = \mathrm{E}_{\Phi_b, G_t}\left[\mathrm{tr}\left(\left(\mathbf{F}_\mathrm{A} + \mathbf{F}_\mathrm{R}\right)^{-1}\right)\right]. \tag{9}$$

C. Cooperative Communication Model

We assume that the transmitters use non-coherent joint transmission, where the useful signals are combined by accumulating their powers. In this work, we employ a user-centric clustering approach, where the BS closest to the typical user sends collaboration requests to other BSs within a range D of the user. The signal received at the typical user located at the origin is then given by

$$y_c = \sum\nolimits_{i \in \Phi_c} d_i^{-\frac{\alpha}{2}} \mathbf{h}_i^H \mathbf{W}_i \mathbf{s}_1 + \sum\nolimits_{j \in \{\Phi_b \setminus \Phi_c\}} d_i^{-\frac{\alpha}{2}} \mathbf{h}_j^H \mathbf{W}_j \mathbf{s}_j + n_c, \tag{10}$$

where $\alpha \geq 2$ is the pathloss exponent, $\mathbf{h}_i^H \sim \mathcal{CN}\left(0, \mathbf{I}_{M_\mathrm{t}}\right)$ is the channel vector of the link between the BS at $\mathbf{d}_i$ to the typical user, Φ_c is the cooperative BS set, and n_c denotes the noise. We focus on evaluating the performance of an interference-limited network within dense cellular scenarios. The impact of noise is disregarded in this analysis. The evaluation is based on the signal-to-interference ratio (SIR) at the typical user, which can be expressed as [19]

$$\mathrm{SIR}_c = \frac{\sum\limits_{i \in \Phi_c} g_i d_i^{-\alpha}}{\sum\limits_{j \in \{\Phi_b \setminus \Phi_c\}} g_j d_i^{-\alpha}}, \tag{11}$$

where $g_1 = p^c \left|\mathbf{h}_1^H \mathbf{w}_1^c\right|^2$ and $g_i = p^c \left|\mathbf{h}_i^H \mathbf{w}_i^c\right|^2$ denotes the desired signals' effective channel gain. The average data rate of users is given by

$$R_c = \mathrm{E}_{\Phi_b, g_i}[\log(1 + \mathrm{SIR}_c)]. \tag{12}$$

III. Sensing Performance Analysis

To facilitate the analysis, we assume that the number of BSs within a range D from each target equals the average number of BSs in the area based on the density of the PPP.

A. Angle Measurement Based Localization

In this subsection, we derive the closed-form CRLB expression under the assumption of random locations of both the BSs and targets. To obtain a tractable CRLB expression with N cooperating BSs, we resort to a simple yet tight approximation. Then the following conclusion is proved.

Proposition 1: The expected CRLB can be approximated as

$$\mathrm{CRLB_A} = \frac{16|\zeta_a|^{-2} \sum_{i=1}^{N} \mathrm{E}[d_i]^{-\beta-2}}{3 \sum_{k=1}^{N} \mathrm{E}[d_k]^{-\beta} \sum_{i=1}^{N} \sum_{i>j}^{N} \mathrm{E}[d_i]^{-\beta-2} \mathrm{E}[d_j]^{-\beta-2}}. \tag{13}$$

Proof: To facilitate the analysis, we transform $\mathrm{CRLB_A}$ in (6) as

$$\begin{aligned} &\mathrm{E}_{\theta,d}\left[\frac{\sum_{i=1}^{N} f_i^2 d_i^{-4}}{\sum_{j=1}^{N} \frac{1}{d_j^2}\left(\sum_{i=1}^{N} \frac{e_i^2}{d_i^4} \sum_{i=1}^{N} \frac{f_i^2}{d_i^4} - \left(\sum_{i=1}^{N} \frac{1}{d_i^4} e_i f_i\right)^2\right)}\right] \\ =&\mathrm{E}_{\theta,d}\left[\frac{\sum_{i=1}^{N} f_i^2 d_i^{-4}}{\sum_{j=1}^{N} \frac{1}{d_j^2}\left(\sum_{i=1}^{N} \sum_{i>j}^{N} \frac{1}{d_i^4 d_j^4} (X_{i,j})^2\right)}\right], \end{aligned} \tag{14}$$

where $X_{i,j} = \sin\theta_i \cos\theta_i \cos^2\theta_j - \sin\theta_j \cos\theta_j \cos^2\theta_i$. Then, we take the expectation over the angle θ, and then substitute the expectation of the distance, resulting in equation (13). ■

Interestingly, we found that the expected CRLB in Proposition 1 is only determined by the expected distance from the BS to the typical target. Furthermore, the expected distance from the nth closest BS to the typical target can be expressed as $E\left[d_n\right] = \frac{\Gamma\left(n+\frac{1}{2}\right)}{\sqrt{\lambda_b \pi \Gamma(n)}} \approx \sqrt{\frac{n}{\lambda_b \pi}}$. Then, the CRLB expression can be further approximated as

$$\mathrm{CRLB_A} \approx \frac{32|\zeta_a|^{-2} \sum_{i=1}^{N} i^{-\frac{\beta}{2}-1}}{3\lambda_b^3 \pi^3 \sum_{k=1}^{N} k^{-\frac{\beta}{2}} \left(\left(\sum_{i=1}^{N} i^{-\frac{\beta}{2}-1}\right)^2 - \sum_{i=1}^{N} i^{-\beta-2}\right)}. \tag{15}$$

For $\beta = 2$, we further derive the scaling law of the localization accuracy as follows.

Theorem 1: For an infinite cooperative cluster size N and fixed $|\zeta_a|$, the expected CRLB of AOA-based localization is given by

$$\lim_{N \to \infty} \mathrm{CRLB_A} \times \ln N = \frac{320}{3|\zeta_a|^2 \lambda_b^3 \pi^5}. \tag{16}$$

Proof: When $\beta = 2$, it follows that

$$\mathrm{CRLB_A} \approx \frac{32|\zeta_a|^{-2}\sum_{i=1}^{N} i^{-2}}{3\lambda_b^3\pi^3\sum_{k=1}^{N} k^{-1}\left(\left(\sum_{i=1}^{N} i^{-2}\right)^2 - \sum_{i=1}^{N} i^{-4}\right)}. \tag{17}$$

Since $\lim_{N\to\infty}\sum_{n=1}^{N}\frac{1}{n} \approx \ln N + \gamma + \frac{1}{2N}$ and $\lim_{N\to\infty}\sum_{n=1}^{N}\frac{1}{n^2} \approx \frac{\pi^2}{6}$, where $\gamma = 0.577$, we get

$$\mathrm{CRLB_A} \approx \frac{320}{3\lambda^3\pi^5\left(\ln N + \gamma + \frac{1}{2N}\right)}. \tag{18}$$

When $N \to \infty$, (16) can be derived. ■

For optimal sensing performance, the transmit beamforming gain can be approximated as $\left\lfloor \frac{\lambda_t D^2 \pi}{N} \right\rfloor$, and the BS density can be expressed by $\frac{N}{\pi D^2}$. Then, we have

$$\mathrm{CRLB_A} \approx \frac{320N}{3|\tilde{\zeta}_a|^2 D^2 \pi^6 \lambda_t \lambda_r \ln N}, \tag{19}$$

where $|\tilde{\zeta}_a|^2 = \frac{1}{6}\pi^2\sigma p^s \gamma_0/\sigma_s^2$. According to (19), as the number of BSs increases significantly, the value of $\mathrm{CRLB_A}$ also increases monotonically with N.

B. Range Measurement Based Localization

In this subsection, we derive the closed-form CRLB expression of the TOF-based localization method. To facilitate the performance analysis, the CRLB expression can be equivalently transformed into

$$\mathrm{CRLB_R} = \mathrm{E}_{\Phi_b}\Bigg[|\zeta_r|^{-2}\times \frac{2\sum_{i=1}^{N}\sum_{j=1}^{N} d_i^{-\beta} d_j^{-\beta}\left(1+\cos\left(\theta_i-\theta_j\right)\right)}{\sum_{l=1}^{N}\sum_{k=1}^{N}\sum_{i\geq k}^{N}\sum_{j>\lceil (k-i)N+l\rceil^+}^{N}\left(d_i d_j d_l d_k\right)^{-\beta} v_{ijkl}^2}\Bigg], \tag{20}$$

where $\lceil x \rceil^+ = \max(x, 1)$ and $v_{ijkl} = a_{kl}b_{ij} - a_{ij}b_{kl}$. For $\beta = 2$, we further derive the scaling law of the localization accuracy as follows.

Theorem 2: For an infinite cooperative cluster size N and fixed $|\zeta_r|$, the expected CRLB is given by

$$\lim_{N\to\infty} \mathrm{CRLB_R} \times \ln^2 N = \frac{2}{|\zeta_r|^2\lambda_b^2\pi^2}. \tag{21}$$

Proof: The proof follows a similar approach to that in Theorem 1. Details are omitted due to space constraints. ■

In the term $|\zeta_R|$, the transmit beamforming gain can be approximated as $\left\lfloor \frac{\lambda_t D^2 \pi}{N} \right\rfloor$. Then, we have

$$\mathrm{CRLB_R} \approx \frac{2}{|\tilde{\zeta}_r|^2\pi^2\lambda_t\lambda_r \ln^2 N}, \tag{22}$$

where $|\tilde{\zeta}_r|^2 = \frac{8\pi^2 p^s B^2 \sigma\gamma_0}{c^2\sigma_s^2}$. According to (22), when the number of BSs is sufficiently large, the $\mathrm{CRLB_R}$ value decreases monotonically as the number of BSs N increases. Therefore, the TOF-based localization method tends to favor a distributed antenna allocation to achieve better sensing results at closer distances.

C. Joint Angle and Range Localization

Under general setup, the CRLB expression can be transformed into (23), as shown at the top of the next page, where $\rho_{ij} = \frac{1}{d_j^2 d_i^2}$, $\tilde{a}_{ij} = \sqrt{\rho_{ij}\left|\zeta_R\right|}\left(\cos\theta_i + \cos\theta_j\right)$, $\tilde{b}_{ij} = \sqrt{\rho_{ij}\left|\zeta_R\right|}\left(\sin\theta_i + \sin\theta_j\right)$, $\tilde{c}_{ij} = \sqrt{\rho_{ij}\left|\zeta_R\right|}\frac{\sin\theta_i\cos\theta_i}{d_i}$, and $\tilde{e}_{i,j} = \sqrt{\rho_{ij}\left|\zeta_R\right|}\frac{\cos^2\theta_i}{d_i}$. To facilitate the analysis, we adopt the following approximation: $E\left[\left(\tilde{a}_{kl}\tilde{b}_{ij} - \tilde{a}_{ij}\tilde{b}_{kl}\right)^2\right]$, $E\left[\left(\tilde{c}_{ij}\tilde{e}_{lk} - \tilde{e}_{lk}\tilde{c}_{ij}\right)^2\right] = \frac{3}{32}\rho_{ij}\rho_{kl}|\zeta_R|^2\frac{1}{d_i^2 d_k^2}$, and $E\left[\left(\tilde{a}_{ij}\tilde{e}_{lk} + \tilde{b}_{lk}\tilde{c}_{ij}\right)^2\right] = \rho_{ij}\rho_{kl}\left|\zeta_R\right|\left|\zeta_A\right|\frac{1}{2d_k^2}$.

Proposition 2: The CRLB of our hybrid localization method is given by

$$\mathrm{CRLB_H} \approx \frac{24}{12\left|\xi_R\right|\lambda_b^2\pi^2\ln^2 N + \lambda_b^3\pi^5\left|\xi_A\right|\ln N}. \tag{24}$$

Proof: The proof follows a similar approach to that in Theorem 1. Details are omitted due to space constraints. ■

IV. Communication Performance

According to [20], for the uncorrelated variables X and Y, it follows that:

$$\mathrm{E}\left[\log\left(1+\frac{X}{Y}\right)\right] = \int_0^\infty \frac{1}{z}\left(1-\mathrm{E}\left[e^{-z[X]}\right]\right)\mathrm{E}\left[e^{-z[Y]}\right]\mathrm{d}z. \tag{25}$$

In (25), $\mathrm{E}\left[e^{-z[X]}\right]$ and $\mathrm{E}\left[e^{-z[Y]}\right]$ are the Laplace transforms of X and Y. Then, exploiting the BSs for cooperative joint transmission within the range D, the expectation of data rate can be expressed as follows:

$$\mathrm{E}\left[\log\left(1+\mathrm{SIR}_c\right)\right] = \mathrm{E}\left[\log\left(1+\frac{\sum_{i\in\Phi_c} g_i\left\|\mathbf{d}_i\right\|^{-\alpha}}{\sum_{j\in\{\Phi_b\setminus\Phi_c\}} g_j\left\|\mathbf{d}_j\right\|^{-\alpha}}\right)\right]$$
$$= \int_0^\infty \frac{1-\mathrm{E}\left[e^{-zU}\right]}{z}\mathrm{E}\left[e^{-zI}\right]\mathrm{d}z, \tag{26}$$

where $U = \sum_{i\in\Phi_c} g_i r^\alpha$ and $I = \sum_{i\in\{\Phi_b\setminus\Phi_c\}} g_i\left\|\mathbf{d}_i\right\|^{-\alpha} r^\alpha$. In (26), I represents the interference arising from the BSs located outside the cooperative region. The term g_i denotes the effective channel gain of the desired signal, where $g_i \sim \Gamma\left(M_\mathrm{t} - 1, p^c\right)$ as described in [8]. According to the definition provided below equation (11), the distribution of g_j can be derived using the moment matching technique [8]. Given that $\mathrm{E}[p^c\left|\mathbf{h}_j^H\mathbf{w}_j^c\right|^2] = p^c$ and $\mathrm{E}[p^s\left|\mathbf{h}_j^H\mathbf{w}_j^s\right|^2] = p^s$, we obtain $\mathrm{E}[g_j] = p^s + p^c = 1$. Moreover, since $\mathrm{E}[g_j^2] = \mathrm{E}\left[\left|\mathbf{h}_j^H\mathbf{w}_j^s\right|^4\right] + \mathrm{E}\left[\left|\mathbf{h}_j^H\mathbf{w}_j^c\right|^4\right] + 2\mathrm{E}\left[\left|\mathbf{h}_j^H\mathbf{w}_j^s\right|^2\left|\mathbf{h}_j^H\mathbf{w}_j^c\right|^2\right] = (p^s + p^c)^2 = 1$,, the interference channel gain g_j can be approximated by a gamma-distributed random variable. Consequently, $g_j \sim \Gamma(1, 1)$.

Based on the above discussions, the useful signal power can be expressed by

$$\mathrm{E}\left[e^{-zg_1}\right] \simeq \int_0^\infty \frac{e^{-zx}x^{M_\mathrm{t}-2}e^{-\frac{x}{p^c}}}{(p^c)^{M_\mathrm{t}-1}\Gamma\left(M_\mathrm{t}-1\right)}\mathrm{d}x = (1+p^c z)^{1-M_\mathrm{t}}. \tag{27}$$

Then, we derive tight bounds on the Laplace transform of the cooperative transmission power and on the communication interference as follows.

$$\mathrm{tr}\left(\left(\mathbf{F}_{\mathrm{A}}+\mathbf{F}_{\mathrm{R}}\right)^{-1}\right)= \frac{\sum_{i=1}^{N}\sum_{j=1}^{N}\left(\tilde{a}_{ij}^{2}+\tilde{c}_{ij}^{2}\right)+\sum_{i=1}^{N}\sum_{j=1}^{N}\left(\tilde{b}_{ij}^{2}+\tilde{e}_{ij}^{2}\right)}{\sum_{l=1}^{N}\sum_{k=1}^{N}\sum_{i\geq k}^{N}\sum_{j>\lceil (k-i)N+l\rceil^{+}}^{N}\left(\left(\tilde{a}_{ij}\tilde{b}_{lk}-\tilde{a}_{lk}\tilde{b}_{ij}\right)^{2}+\left(\tilde{c}_{ij}\tilde{e}_{lk}-\tilde{e}_{lk}\tilde{c}_{ij}\right)^{2}\right)+\sum_{l=1}^{N}\sum_{k=1}^{N}\sum_{i=1}^{N}\sum_{j=1}^{N}\left(\tilde{a}_{ij}\tilde{e}_{lk}+\tilde{b}_{lk}\tilde{c}_{ij}\right)^{2}}. \tag{23}$$

Lemma 1: The Laplace transforms of U and I are given by

$$\mathrm{E}\left[e^{-zU}\right]=\exp\left(-\pi\lambda_b\mathrm{H}_1\left(zp^c,M_{\mathrm{t}}-1,\alpha,D\right)\right), \tag{28}$$

$$\mathrm{E}\left[e^{-zI}\right]=\exp\left(-\pi\lambda_b\mathrm{H}_2\left(z,\alpha,D\right)\right), \tag{29}$$

where $\mathrm{H}_1\left(x,K,\alpha,D\right)=Kx^{\frac{2}{\alpha}}\bar{B}\left(\frac{x}{x+D^{\alpha}},1-\frac{2}{\alpha},K+\frac{2}{\alpha}\right)+D^2\left(1-\left(1+xD^{-\alpha}\right)^{-K}\right)$ and $\mathrm{H}_2\left(x,\alpha,D\right)=D^2\left(\left(1+xD^{-\alpha}\right)^{-K}-1\right)+Kx^{\frac{2}{\alpha}}B\left(\frac{x}{x+D^{\alpha}},1-\frac{2}{\alpha},K+\frac{2}{\alpha}\right)$. $B(a,b,c)=\int_0^a t^{b-1}(1-t)^{c-1}dt$ and $\bar{B}(a,b,c)=\int_a^1 t^{b-1}(1-t)^{c-1}dt$ are the lower and upper incomplete Beta function, respectively.

Proof: For the Laplace transform of the interference coming from the BSs outside the cooperative region, we have

$$\begin{aligned}\mathcal{L}_I(z)=&\mathrm{E}_{\Phi_b,g_i}\left[\exp\left(-z\sum\nolimits_{i\in\Phi_b}\|\mathbf{d}_i\|^{-\alpha}|\mathbf{h}_i^H\mathbf{W}_i|^2\right)\right]\\ \overset{(a)}{=}&\mathrm{E}_{\Phi_b}\left[\left(\prod_{\mathbf{d}_i\in\Phi_b\setminus\mathcal{O}(0,D)}\left(1+z\|\mathbf{d}_i\|^{-\alpha}\right)^{-1}dx\right)\middle|D\right]\\ \overset{(b)}{=}&\exp\left(-2\pi\lambda_b\int_D^{\infty}\left(1-\left(1+zx^{-\alpha}\right)^{-1}\right)xdx\right)\\ \overset{(c)}{=}&\exp\Bigg(-\pi\lambda_b y\left(1-\left(1+zy^{-\frac{\alpha}{2}}\right)^{-1}\right)\Big|_{D^2}^{\infty}\\ &-\pi\lambda_b\int_{D^2}^{\infty}\frac{\alpha}{2}zy^{-\frac{\alpha}{2}}\left(1+zy^{-\frac{\alpha}{2}}\right)^{-2}dy\Bigg).\end{aligned} \tag{30}$$

In (30), (a) follows from the fact that the small-scale channel fading is independent of the BS locations and that the interference power imposed by each interfering BS at the typical user is distributed as $\Gamma(1,1)$. To derive (b), we harness the probability generating functional of a PPP with density λ_b. To elaborate, (c) comes from the variable $y=x^2$ and the distribution integral strategies. Then, we have

$$\int_0^{zr^{-\alpha}}(1+u)^{-K-1}u^{-\frac{2}{\alpha}}du\overset{(d)}{=}B\left(\frac{zr^{-\alpha}}{1+zr^{-\alpha}},1-\frac{2}{\alpha},K+\frac{2}{\alpha}\right), \tag{31}$$

where (d) in (31) follows from the distribution integral strategies and $u=\frac{x}{1-x}$. Similarly, the Laplace transform of useful signals can be derived. This completes the proof. ■

Based on the Laplace transforms of U and I in (28) and (29), the expected data rate is formulated in Theorem 3.

Theorem 3: The communication performance is characterized by

$$R_c=\int_0^{\infty}\frac{1-\exp\left(-\pi\lambda_b\mathrm{H}_1\left(zp^c,M_{\mathrm{t}}-1,\alpha,D\right)\right)}{z}\times\exp\left(-\pi\lambda_b\mathrm{H}_2\left(z,\alpha,D\right)\right)\mathrm{d}z, \tag{32}$$

where $\lambda_b=\lambda_t/M_{\mathrm{t}}$.

Proof: According to (25), by substituting the Laplace transforms of useful signal and interference in Lemma 1 into (26), the conditional expected spectrum efficiency is given by

$$\int_0^{\infty}\int_0^{\infty}\frac{1-\exp\left(-\pi\lambda_b\mathrm{H}_1\left(zp^c,M_{\mathrm{t}}-1,\alpha,D\right)\right)}{z}\times\exp\left(-\pi\lambda_b\mathrm{H}_2\left(z,\alpha,D\right)\right)f_r\left(r\right)\mathrm{d}r\mathrm{d}z, \tag{33}$$

where we have $f_r\left(r\right)=2\pi\lambda_b re^{-\pi\lambda_b r^2}$. Then, by solving the integral with respect to r, (32) can be obtained. This completes the proof. ■

According to (32), the communication rate increases monotonically with the increase of D, which is due to having on average more BSs participating in cooperative transmission, while users receive less interference.

V. Simulations

Using numerical results, we study the fundamental insights of ISAC networks and verify the tightness of the derived tractable expression by comparing with Monte Carlo simulation results in this section. The system parameters are given as follows: the number of transmit antennas $M_{\mathrm{t}}=4$; the number of receive antennas $M_{\mathrm{r}}=10$; the transmit power $P_{\mathrm{t}}=1$W at each BS; $|\xi|^2=1$, the transmit and receive antenna density $\lambda_t=\lambda_r=50/\mathrm{km}^2$; the frequency $f^c=5$ GHz; the bandwidth $B\in[10,100]$ MHz; the noise power -100dB; pathloss coefficients $\alpha=4$ and $\beta=2$.

In Fig. 2, given $M_t=4$ and $M_r=10$, and bandwidth $B=10$ MHz, the scaling law of the CRLB expressions derived in Theorems 1, 2, and Proposition 2 are also consistent with the simulation results. When the number of BSs is small, the hybrid localization method can significantly improve performance. This is primarily because the geometric arrangement of the BSs relative to the target may be suboptimal, leading to poor performance in localization methods that rely solely on ranging or AOA measurements. Fig. 2 shows that increasing the number of cooperative BSs significantly improves accuracy when the total number of BSs is limited. However, the performance gains become marginal once $N\geq 10$. This is expected, as adding more distant and randomly located BSs leads to increased signal attenuation, offering diminishing returns compared to nearby BSs. Additionally, hybrid localization, which combines TOF and AOA estimation results, can greatly enhance accuracy when the number of BSs is small.

In Fig. 3, both the transmit and receive antenna densities are set at $\lambda_t=\lambda_r=50/\mathrm{km}^2$. The noise power is $\sigma_s^2=-100$ dB, and the bandwidth is $B=10$ MHz. Consistent with our

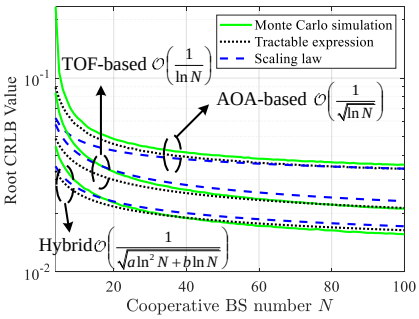

Fig. 2. Localization performance scaling law with respect to the cooperative BS number N under the fixed number of antennas per BS.

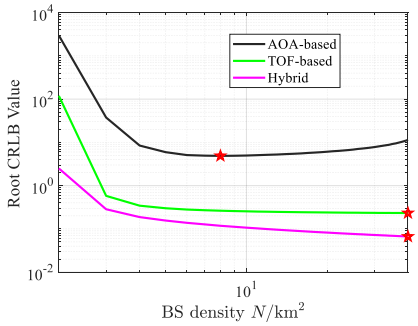

Fig. 3. Localization performance comparisons with respect to the cooperative BS density under the fixed antenna density

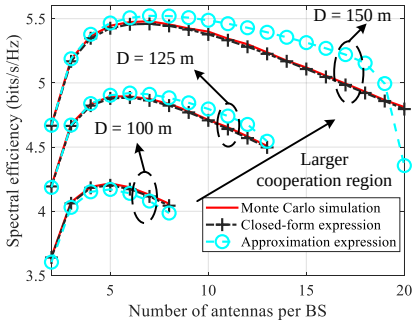

Fig. 4. Antenna allocation versus spectrum efficiency with different cooperative ranges D = 100, 125, and 150 m.

analysis, Fig. 3 shows that the optimal allocation strategy for TOF-based and hybrid localization methods is a fully distributed configuration. By contrast, for AOA-based localization, the optimal allocation requires concentrating a certain number of antennas to improve the AOA estimation accuracy, resulting in an ideal allocation of eight BSs per square kilometer. Fig. 4 shows that our derived tractable expression for the communication rate closely aligns with the Monte Carlo simulations, given an antenna density of $\lambda_t = 300/\text{km}^2$. Fig. 4 also shows that spectral efficiency R_c initially increases with the number of antennas per BS but then decreases. This is because the initial improvement in communication performance from beamforming gain is eventually outweighed by the performance loss resulting from the increased average serving distance, which is due to the reduced BS density. As the radius D of the cooperative area expands, the optimal communication rate increases, mainly due to the higher signal power and reduced interference power. Additionally, with a larger cooperative area, the optimal number of antennas per BS also rises to maximize communication rates. This is because a larger area provides more antenna resources, and adding antennas at each BS improves beamforming gain, which helps mitigate the path loss associated with the expanded cooperative area.

VI. Conclusions

This work proposed an innovative cooperative ISAC network that combines multi-static sensing with CoMP data transmission, incorporating advanced localization methods that exploit both AOA and TOF measurements. Our study demonstrates that optimal antenna-to-BS allocation, through a balance of centralized and distributed configurations, significantly enhances network performance by maximizing spatial diversity and coherent processing gains. We provide analytical insights into the scaling laws of different localization techniques and establish a comprehensive framework for evaluating communication data rates.

References

[1] X. Liu *et al.*, "Joint transmit beamforming for multiuser MIMO communications and MIMO radar," *IEEE Trans. Signal Process.*, vol. 68, pp. 3929–3944, 2020.

[2] K. Meng, Q. Wu, W. Chen, and D. Li, "Sensing-assisted communication in vehicular networks with intelligent surface," *IEEE Trans. Veh. Technol.*, vol. 73, no. 1, pp. 876–893, 2024.

[3] Y. Cui, F. Liu, X. Jing, and J. Mu, "Integrating sensing and communications for ubiquitous IoT: Applications, trends, and challenges," *IEEE Net.*, vol. 35, no. 5, pp. 158–167, Sep./Oct. 2021.

[4] C. Ouyang, Y. Liu, and H. Yang, "Performance of downlink and uplink integrated sensing and communications (ISAC) systems," *IEEE Wireless Commun. Lett.*, vol. 11, no. 9, pp. 1850–1854, Sep. 2022.

[5] F. Liu, Y. Cui, C. Masouros, J. Xu, T. X. Han, Y. C. Eldar, and S. Buzzi, "Integrated sensing and communications: Towards dual-functional wireless networks for 6G and beyond," *IEEE J. Sel. Areas Commun.*, vol. 40, no. 6, pp. 1728–1767, Jun. 2022.

[6] R. Li, Z. Xiao, and Y. Zeng, "Toward seamless sensing coverage for cellular multi-static integrated sensing and communication," *IEEE Trans. Wireless Commun.*, vol. 23, no. 6, pp. 5363–5376, 2024.

[7] K. Meng *et al.*, "Network-level integrated sensing and communication: Interference management and BS coordination using stochastic geometry," *arXiv preprint arXiv:2311.09052*, 2023.

[8] K. Hosseini, W. Yu, and R. S. Adve, "A stochastic analysis of network MIMO systems," *IEEE Trans. Signal Process.*, vol. 64, no. 16, pp. 4113–4126, Aug. 2016.

[9] K. Meng, C. Masouros, A. P. Petropulu, and L. Hanzo, "Cooperative ISAC networks: Performance analysis, scaling laws and optimization," *arXiv preprint arXiv:2404.14514*, 2024.

[10] A. Salem *et al.*, "Rethinking dense cells for integrated sensing and communications: A stochastic geometric view," *IEEE Open J. Commun. Society*, vol. 5, pp. 2226–2239, 2024.

[11] T. S. Rappaport, Y. Xing, G. R. MacCartney, A. F. Molisch, E. Mellios, and J. Zhang, "Overview of millimeter wave communications for fifth-generation (5G) wireless networks-with a focus on propagation models," *IEEE Trans. Antennas Propag.*, vol. 65, no. 12, pp. 6213–6230, 2017.

[12] H. Q. Ngo, A. Ashikhmin, H. Yang, E. G. Larsson, and T. L. Marzetta, "Cell-free massive MIMO versus small cells," *IEEE Trans. Wireless Commun.*, vol. 16, no. 3, pp. 1834–1850, 2017.

[13] J. G. Andrews, F. Baccelli, and R. K. Ganti, "A tractable approach to coverage and rate in cellular networks," *IEEE Trans. Commun.*, vol. 59, no. 11, pp. 3122–3134, Nov. 2011.

[14] J. Li and P. Stoica, *MIMO radar signal processing*. John Wiley & Sons, 2008.

[15] J. Li and R. Compton, "Maximum likelihood angle estimation for signals with known waveforms," *IEEE Trans. Signal Process.*, vol. 41, no. 9, pp. 2850–2862, 1993.

[16] M. A. Richards *et al.*, *Fundamentals of radar signal processing*. Mcgraw-hill New York, 2005, vol. 1.

[17] A. Liu *et al.*, "A survey on fundamental limits of integrated sensing and communication," *IEEE Commun. Surveys Tuts.*, vol. 24, no. 2, pp. 994–1034, Nov. 2022.

[18] M. Sadeghi, F. Behnia, R. Amiri, and A. Farina, "Target localization geometry gain in distributed MIMO radar," *IEEE Trans. Signal Process.*, vol. 69, pp. 1642–1652, 2021.

[19] J. Park *et al.*, "On the optimal feedback rate in interference-limited multi-antenna cellular systems," *IEEE Trans. Wireless Commun.*, vol. 15, no. 8, pp. 5748–5762, Aug. 2016.

[20] K. A. Hamdi, "A useful lemma for capacity analysis of fading interference channels," *IEEE Trans. Commun.*, vol. 58, no. 2, pp. 411–416, Feb. 2010.